NANO LETTERS

pubs.acs.org/NanoLett

Semitransparent Organic Photovoltaic Cells with Laminated Top Electrode

Jung-Yong Lee,[†] Steve T. Connor,[‡] Yi Cui,[§] and Peter Peumans*[,†]

[†]Department of Electrical Engineering, [‡]Department of Chemistry, and [§]Department of Materials Science and Engineering, Stanford University, Stanford, California 94305

ABSTRACT We demonstrate semitransparent small molecular weight organic photovoltaic cells using a laminated silver nanowire mesh as a transparent, conductive cathode layer. The lamination process does not damage the underlying solar cell and results in a transparent electrode with low sheet resistance and high optical transmittance without impacting photocurrent collection. The resulting semitransparent phthalocyanine/fullerene organic solar cell has a power conversion efficiency that is 57% of that of a device with a conventional metal cathode due to differences in optical absorption.

KEYWORDS Organic photovoltaics, transparent electrodes, nanowires

Organic photovoltaic cells are considered a promising solar cell technology because of the tunability of the electronic and optical properties of organic semiconductors and the potential for low-cost roll-to-roll manufacturing. However, the relatively low efficiency of organic solar cells is a major roadblock that stands in the way of commercialization. A plausible path toward higher conversion efficiencies is the use of multijunction cell architectures where several individual cells with different optical gaps are combined into a series-connected stack,[1−3] as shown in Figure 1a. However, the requirement that each cell in the series-connected stack produce the same photocurrent, limits this approach. This is especially the case when an optimized material system[4] is combined with one that is not yet optimized, or when the energy gaps of the materials are not ideal. In multijunction architectures in which the cells are individually accessible and photocurrent matching is not required, as shown in Figure 1b, higher efficiencies can be achieved[4] for a given number of subcells. Such an arrangement requires a transparent conductor[5−13] between adjacent subcells that makes an ohmic contact to both subcells while being transparent and conductive in the plane to ensure that current can be extracted without ohmic losses. Furthermore, this electrode must be deposited on top of an organic solar cell without incurring damage to the underlying cell. Here, we describe such an electrode that satisfies all the above requirements.

A transparent polymer cathode that can be laminated on top of an organic photovoltaic cell was previously reported,[14] but device performance suffered due to the relatively low conductivity (10^2∼10^3 S/cm) of the polymer layer. Indium−tin−oxide (ITO) transparent cathode layers sputter-deposited at low plasma powers and hence low deposition rates have also been used.[15,16] However, the slow and therefore expensive sputtering process used is undesirable and damages the underlying organic active layer leading to lower device performance.[17] Thin, semitransparent metal films have been used as transparent electrodes and exhibit good performance, albeit not identical to sputter-coated ITO, if optical interference effects can be exploited.[7,18,19] In multijunction configurations, the additional reflections of the metal films are likely to substantially complicate cell design. Nanoimprinted metal gratings have been shown to work well as transparent electrodes,[5] but it is unclear whether their cost is sufficiently low.

We reported earlier that solution-processed silver nanowire (NW) meshes have a figure of merit as a transparent conductor on the anode side that is equal or better than that of sputter-coated ITO.[20] With their potentially very low processing and materials cost, silver NW transparent electrodes are attractive for large area applications and roll-to-roll processing. In this letter, we demonstrate that solution-processed silver NW meshes can also be used as high-performance transparent electrodes on top of organic solar cells by a simple, dry lamination step, resulting in a semitransparent solar cell, as shown in Figure 1c. This is a first step toward a multijunction cell unencumbered by current-matching.

Conductive, transparent meshes of silver NWs were prepared on glass substrates as described earlier.[20] Briefly, Ag nanowires were synthesized by the reduction of Ag nitrate in the presence of poly(vinyl pyrrolidone) (PVP) in ethylene glycol.[21] The resulting Ag nanowires are (8.7 ± 3.7) μm long and have a diameter of (103 ± 17) nm. Glass substrates were cleaned by sequential ultrasonic rinses in detergent solution and deionized water, then boiled in trichloroethylene, rinsed in acetone, and finally boiled in 2-propanol. Subsequently, the clean substrates were dipped

* To whom correspondence should be addressed. E-mail: ppeumans@stanford.edu.

Received for review: 11/20/2009
Published on Web: 03/30/2010

DOI: 10.1021/nl903892x | *Nano Lett.* **2010,** *10,* 1276–1279

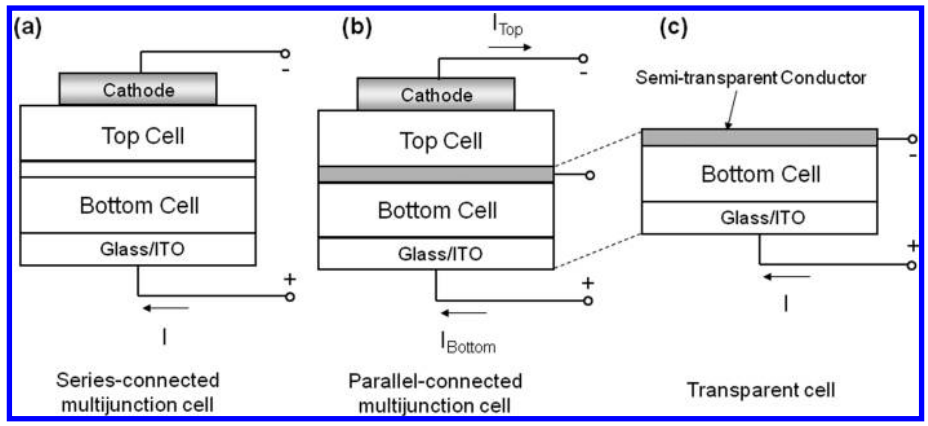

FIGURE 1. (a) Conventional tandem structure with recombination layer, which requires photocurrent matching throughout the device. (b) Tandem structure with intermediate electrode, in which each cell can be operated independently. (c) Semitransparent photovoltaic cell structure. Both electrodes need to be transparent and conductive in-plane.

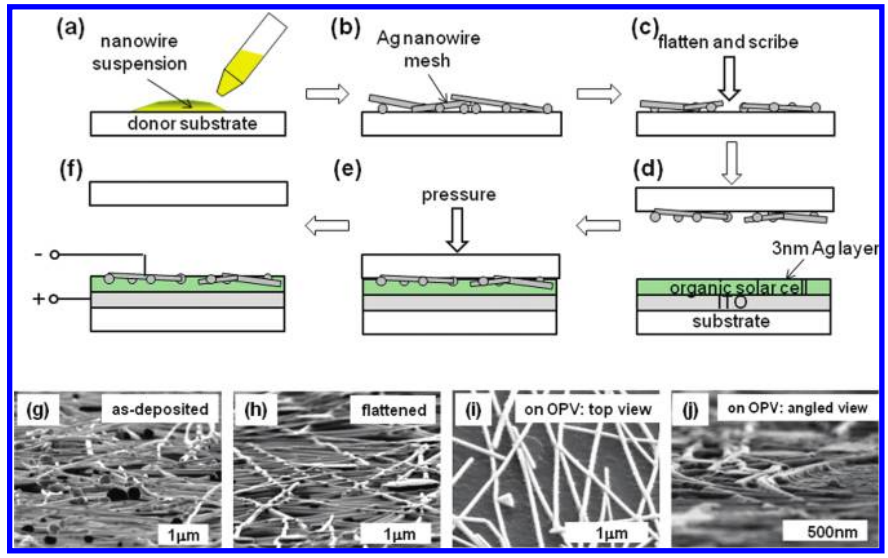

FIGURE 2. (a−f) Schematic illustration of the fabrication process. (g−j) Scanning electron microscope images of (g) Ag nanowires as-deposited on a glass substrate recorded 85° off-normal before and (h) after application of 10^4 psi uniaxial pressure was applied. (i) Complete semitransparent photovoltaic cell seen from the normal direction, and (j) from 85° off-normal.

in an aqueous poly-L-lysine solution (0.1% w/v, Ted Pella) for 5 min, rinsed with deionized water and blown with N_2 gas. A volume of the nanowire suspension was then dropped onto a cleaned glass substrate coated with poly L-lysine and was allowed to dry in air for 10 min (Figure 2a). The affinity of the Ag NWs for poly-L-lysine, prevents the NWs from aggregating while the suspension dries on the substrate (Figure 2b). The meshes are subsequently heated to 180 °C for 20 min to allow the NWs to fuse together.[20] The resulting silver NW meshes have a sheet resistance of 15−25 Ω/square and solar-averaged transmission of 75−85% and are relatively rough with protrusions as high as 200−300 nm, as shown in the glancing-angle (85° off-normal) scanning electron micrograph (SEM) in Figure 2g. These films are too rough for use in most organic solar cells with active layer thicknesses in the range of 50−200 nm. To lower the surface roughness, the NW meshes were subjected to a $(1.4 \pm 0.6) \times 10^4$ psi uniaxial pressure applied via a clean glass substrate, using a hydraulic press for 30 s, leading to substantial flattening of the features as shown in Figure 2h. The poly-L-lysine adhesive layer prevents the nanowires from being transferred to the uncoated glass substrate. The silver NW meshes were then patterned using a razor blade to define the electrode patterns (Figure 2c). Conventional small molecular weight organic solar cell structures with layer structure 25 nm copper phthalocyanine (CuPc)/50 nm C_{60}/10 nm bathocuproine (BCP)/3 nm Ag were grown on cleaned glass substrates precoated with ITO (∼15 Ω/sq, 130 nm thick). The 3 nm thick evaporated Ag layer is required to ensure an ohmic contact. It was shown that vacuum deposition of Ag leads to the formation of a thin region at the BCP/Ag interface that ensures facile electron transport, presumably through defect states.[2] Such a thin Ag layer does not form a continuous layer and provides no in-plane conductivity. The Ag NW mesh electrode is then laminated onto the organic solar cell structure under a pressure of $(1.4 \pm 0.6) \times 10^4$ psi

DOI: 10.1021/nl903892x | Nano Lett. 2010, 10, 1276–1279

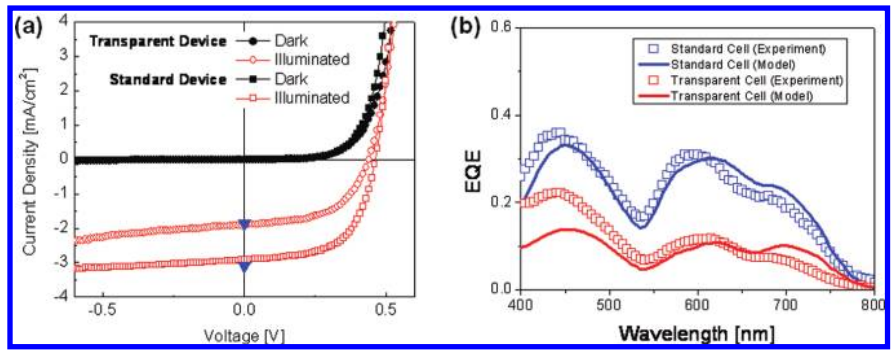

FIGURE 3. (a) Current−voltage characteristics for a semitransparent (circles) and standard cell (squares) in the dark (filled symbols) and under 73mW/cm^2 AM1.5 illumination (open symbols). The modeled short circuit currents for both cells are shown for comparison (triangles). (b) Measured EQE of both a standard and semitransparent organic photovoltaic cell (square markers). The modeled EQE (solid lines) is plotted for comparison.

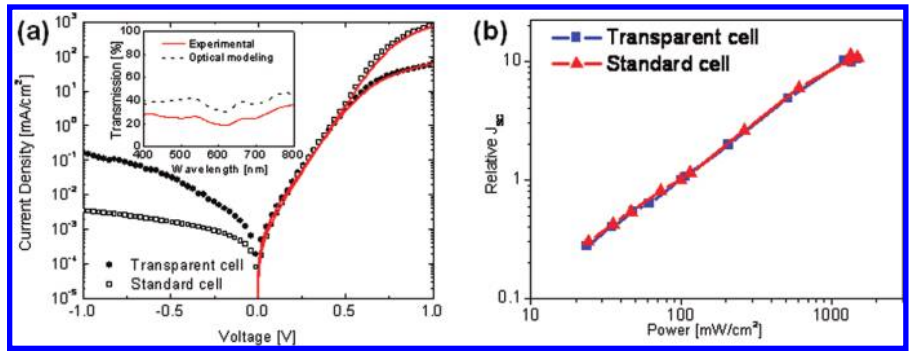

FIGURE 4. (a) Current−voltage characteristics for a semitransparent (filled circles) and standard (open squares) device in the dark on a logarithmic scale. (Inset) Measured transmission spectrum for a semitransparent device (solid line) compared to a model calculation (dashed line). (b) Normalized (to the value obtained at 100 mW/cm^2) short circuit current of both a standard (triangles) and semitransparent (squares) organic photovoltaic cell as a function of illumination intensity. Both cells show a linear dependence on illumination intensities up to 1500mW/cm^2.

for 30 s (Figure 2d,e).This process leads to a complete transfer of the patterned Ag NW mesh from the donor glass substrate to the organic solar cell (Figure 2f). Figure 2i is a top view SEM image of the transferred Ag NW mesh. The SEM image of Figure 2j was taken at a glancing angle (85° off normal), showing that the Ag NW mesh is partially embedded into the underlying organic solar cell structure, possibly contributing to a good electrical contact between the silver NW mesh and the topmost organic layer. Control devices with a vacuum-deposited 100 nm thick Ag cathode were also fabricated in parallel. The fabricated photovoltaic cells were characterized in the dark and under AM1.5G solar illumination. The device areas used were 1 mm^2 for the semitransparent devices and 0.8 mm^2 for the standard devices.

The current density−voltage (J−V) characteristics of a semitransparent (circles) and conventional opaque cell (squares) under 73mW/cm^2 AM1.5 illumination (open symbols) and in the dark (filled symbols) are shown in Figure 3a. The semitransparent cell exhibits a power conversion efficiency (PCE) of 0.63 %, an open circuit voltage of V_{OC} = 0.44 V, a short-circuit current density of J_{SC} = 1.91 mA/cm^2, and a fill factor of FF = 0.55. For comparison, the opaque control device yields PCE = 1.1 %, V_{OC} = 0.46 V, J_{SC} = 2.91 mA/cm^2, and FF = 0.60.

The higher short-circuit current density of the conventional opaque device is attributed to the higher optical absorption in that structure because incident light passes twice through the active layer with additional benefits from optical interference effects.[2] As a first order approximation, we used the transfer matrix formalism to estimate optical absorption, and the exciton diffusion equation in both active layers were solved to predict the external quantum efficiency (EQE) and J_{SC} for both structures, assuming exciton diffusion lengths of 7 nm for CuPc and 15 nm for C_{60}.[2] In the inset of Figure 4a, the measured specular transmittance of the semitransparent organic photovoltaic cells is shown (solid line) and compared to model calculations (dashed line). Since numerical modeling the transmission of random Ag NW meshes is challenging, we modeled the Ag NW mesh as a 10 nm thick Ag film. When averaged over the spectral range 400−800 nm, an average transmission of 26 % is obtained experimentally. The experimentally measured transmission is lower than that predicted by the model. This is attributed to additional diffuse transmittance that was not recorded here. As reported earlier,[20] approximately 20 % of

DOI: 10.1021/nl903892x | Nano Lett. 2010, 10, 1276–1279

the transmitted light is scattered over angles >10°. Figure 3b shows the measured EQE of both a standard and semitransparent organic photovoltaic cell (square markers). The modeled EQE (solid lines) is plotted for comparison. The experimental EQE exceeds the predicted value for $\lambda = 450$ nm. This is attributed to light scattering by the silver nanowire mesh that results in enhanced optical absorption by the active materials. The silver nanowires are indeed projected to have a resonance slightly above 400 nm where C_{60} absorbs strongly. The modeled J_{SC} for the standard and semitransparent devices, obtained by AM1.5-weighting the modeled EQE, are shown in Figure 3a (blue-filled triangles).

In Figure 4a, the dark $J-V$ characteristics of the semitransparent (filled circles) and standard cell (open squares) are shown on a logarithmic scale. The semitransparent cell has a higher leakage current in reverse bias, attributed to locally thinner active regions corresponding to the thickest regions of the silver NW mesh. In the forward direction, the semitransparent device is more resistive. The $J-V$ characteristics were fit to

$$J = J_0\left[\exp\left(\frac{q(V - JR_s)}{nkT}\right) - 1\right] \quad (1)$$

The saturation current density, J_0, is $(5 \pm 2) \times 10^4$ and $(8 \pm 2) \times 10^4$ mA/cm^2 for the standard and semitransparent device, respectively. The ideality factor, n, is (2.15 ± 0.05) and (2.30 ± 0.05) for the standard and semitransparent device, respectively, indicating that the forward current is a recombination current. The series resistance, R_s, is (0.26 ± 0.02) and (5 ± 1) Ωcm^2 for the standard and semitransparent device, respectively. The higher series resistance for the semitransparent device is attributed to the longer average distance electrons have to travel in the in-plane direction within the organic layers to reach a silver NW.

Figure 4b shows the normalized short-circuit photocurrent as a function of illumination intensity for both a standard and semitransparent cell measured using a HeNe laser. The short-circuit current was normalized to that obtained under 100 mW/cm^2. Even at high light intensities ($\sim$1500 mW/cm^2), there is no evidence for significant space-charge build-up which would result in enhanced carrier recombination and a sublinear dependence of the short circuit current on illumination intensity. We conclude that the silver NW mesh cathode does not result in an increased barrier to charge collection compared to a standard silver cathode. The increased series resistance observed for the semitransparent devices does hence not limit the cell performance under concentrated illumination.

In conclusion, we demonstrated semitransparent organic photovoltaic cells that use a laminated Ag NW mesh as a high-performance transparent cathode layer that can be deposited without damaging the underlying organic solar cell. A power conversion efficiency that is 57% of a standard device under simulated AM1.5G illumination and 26% average optical transmittance were demonstrated. Since silver NW meshes can be used as an anode contact in organic solar cells,[20] multijunction structures with highly conductive and transparent metal NW intermediate electrodes are now possible. Because of the additional freedom in design of the individual cells, this may lead to higher efficiency organic multijunction photovoltaic cells unencumbered by current-matching limitations.

Acknowledgment. The authors acknowledge support from the National Science Foundation, the Global Climate and Energy Project at Stanford, and the Department of Energy. J.Y.L. would like to thank The Korea Foundation for Advanced Studies for its support. S.T.C. acknowledges support from an NSF Graduate Fellowship.

REFERENCES AND NOTES

(1) Dennler, G.; Scharber, M. C.; Ameri, T.; Denk, P.; Forberich, K.; Waldauf, C.; Brabec, C. J. *Adv. Mater.* **2008**, *20* (3), 579–583.
(2) Peumans, P.; Yakimov, A.; Forrest, S. R. *J. Appl. Phys.* **2003**, *93* (7), 3693–3723.
(3) Yakimov, A.; Forrest, S. R. *Appl. Phys. Lett.* **2002**, *80* (9), 1667–1669.
(4) Hadipour, A.; de Boer, B.; Blom, P. W. M. *Adv. Funct. Mater.* **2008**, *18* (2), 169–181.
(5) Kang, M.-G.; Guo, L. J. *Adv. Mater.* **2007**, *19* (10), 1391–1396.
(6) Klauk, H.; Huang, J.-R.; Nichols, J. A.; Jackson, T. N. *Thin Solid Films* **2000**, *366* (1−2), 272–278.
(7) O'Connor, B.; Haughn, C.; An, K.-H.; Pipe, K. P.; Shtein, M. *Appl. Phys. Lett.* **2008**, *93* (22), 223304–3.
(8) Li, Y. Q.; Tang, J. X.; Xie, Z. Y.; Hung, L. S.; Lau, S. S. *Chem. Phys. Lett.* **2004**, *386* (1−3), 128–131.
(9) O'Connor, B.; An, K. H.; Pipe, K. P.; Zhao, Y.; Shtein, M. *Appl. Phys. Lett.* **2006**, *89* (23), 233502–3.
(10) Rowell, M. W.; Topinka, M. A.; McGehee, M. D.; Prall, H. J.; Dennler, G.; Sariciftci, N. S.; Hu, L. B.; Gruner, G. *Appl. Phys. Lett.* **2006**, *88* (23), 233506.
(11) Tvingstedt, K.; Inganas, O. *Adv. Mater.* **2007**, *19* (19), 2893–2897.
(12) Yang, F.; Forrest, S. R. *Adv. Mater.* **2006**, *18* (15), 2018–2022.
(13) Zhou, Y.; Zhang, F.; Tvingstedt, K.; Barrau, S.; Li, F.; Tian, W.; Inganas, O. *Appl. Phys. Lett.* **2008**, *92* (23), 233308–3.
(14) Gadisa, A.; Tvingstedt, K.; Admassie, S.; Lindell, L.; Crispin, X.; Andersson, M. R.; Salaneck, W. R.; Inganäs, O. *Synth. Met.* **2006**, *156* (16−17), 1102–1107.
(15) Bailey-Salzman, R. F.; Rand, B. P.; Forrest, S. R. *Appl. Phys. Lett.* **2006**, *88* (23), 233502–3.
(16) Ng, G.-M.; Kietzke, E. L.; Kietzke, T.; Tan, L.-W.; Liew, P.-K.; Zhu, F. *Appl. Phys. Lett.* **2007**, *90* (10), 103505–3.
(17) Gu, G.; Bulovic, V.; Burrows, P. E.; Forrest, S. R.; Thompson, M. E. *Appl. Phys. Lett.* **1996**, *68* (19), 2606–8.
(18) Meiss, J.; Riede, M. K.; Leo, K. *Appl. Phys. Lett.* **2009**, *94* (1), No. 013303−3.
(19) Meiss, J.; Riede, M. K.; Leo, K. *J. Appl. Phys.* **2009**, *105* (6), No. 063108−5.
(20) Lee, J.-Y.; Connor, S. T.; Cui, Y.; Peumans, P. *Nano Lett.* **2008**, *8* (2), 689–692.
(21) Tao, A.; Kim, F.; Hess, C.; Goldberger, J.; He, R.; Sun, Y.; Xia, Y.; Yang, P. *Nano Lett.* **2003**, *3* (9), 1229–1233.

DOI: 10.1021/nl903892x | *Nano Lett.* **2010,** *10,* 1276–1279